Chemical Science

ROYAL SOCIETY OF CHEMISTRY

EDGE ARTICLE

Cite this: *Chem. Sci.*, 2023, **14**, 179

All publication charges for this article have been paid for by the Royal Society of Chemistry

Received 18th September 2022
Accepted 22nd November 2022

DOI: 10.1039/d2sc05192c

rsc.li/chemical-science

Heterometallic palladium–iron metal–organic framework as a highly active catalyst for cross-coupling reactions†

Eugenia Miguel-Casañ,‡[a] Mohanad D. Darawsheh,‡[a] Víctor Fariña-Torres,[b] Iñigo J. Vitórica-Yrezábal,[c] Eduardo Andres-Garcia,[a] Martín Fañanás-Mastral *[b] and Guillermo Mínguez Espallargas *[a]

Palladium-based metal–organic frameworks (Pd-MOFs) are an emerging class of heterogeneous catalysts extremely challenging to achieve due to the facile leaching of palladium and its tendency to be reduced. Herein, Pd(II) was successfully incorporated in the framework of a MOF denoted as **MUV-22** using a solvent assisted reaction. This stable MOF, with square-octahedron (soc) topology as MIL-127, and a porosity of 710 $m^2\ g^{-1}$, is highly active, selective, and recyclable for the Suzuki–Miyaura allylation of aryl and alkyl boronates as exemplified with the coupling between cinnamyl bromide and Me-Bpin, a typically reluctant reagent in cross-coupling reactions.

Introduction

Pd(II) complexes are widely used as homogeneous catalysts in important reactions such as hydrogenation,[1] coupling reactions (both carbon–carbon and carbon–heteroatoms),[2] and photo-hydrogen production reactions,[3] among others. However, given the high cost, the drawbacks related to the recyclability of homogeneous palladium complexes, and deactivation through Pd-black formation, the search of novel heterogeneous catalysts which can be recycled is of high interest.[4,5] Metal–organic frameworks (MOFs), crystalline porous solids composed of metal ions or metal clusters interconnected by organic linkers, are ideal tunable platforms acting as a supporting matrix for the incorporation of catalytically active metals.[6,7] Indeed, MOFs have proven to be very efficient catalysts for a large number of reactions.[8–11] In this sense, MOFs containing palladium atoms (Pd-MOFs) are currently attracting tremendous interest,[12–14] as they can provide a good dispersion of the exposed Pd atoms within the framework, are able to stabilize reaction intermediates,[15] and promote and increase the catalytic activity.[16]

The incorporation of Pd atoms into MOFs has been typically achieved through post-synthetic approaches, *i.e.* in a two-step procedure after the formation of the MOF.[17,18] The most common route consists in the encapsulation of Pd nanoparticles in the pores of the MOFs (Fig. 1a), yielding stable and disperse Pd nanoparticles and avoiding their aggregation and growth,[19,20] but with the limitation of blocking the channels of the MOF. An alternative approach is the use of organic ligands with anchoring groups suitable for the coordination of metal complexes (Fig. 1b),[21,22] which has also proven successful in

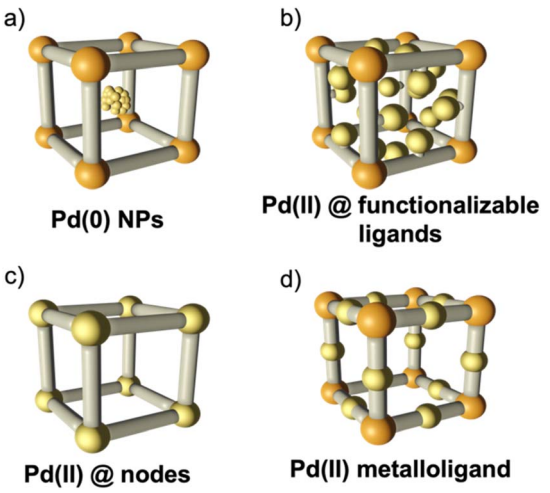

Fig. 1 Catalytically active palladium can be incorporated in a MOF structure by: (a) nanoparticle encapsulation; and using (b) functionalizable ligands; (c) palladium nodes and (d) palladium metalloligands (this work). Color scheme: orange balls = any SBU, yellow ball = Pd.

[a]*Instituto de Ciencia Molecular (ICMol), Universidad de Valencia, C/ Catedrático José Beltrán, 2, 46980, Paterna, Spain. E-mail: guillermo.minguez@uv.es*

[b]*Centro Singular de Investigación en Química Biolóxica e Materiais Moleculares (CiQUS), Universidade de Santiago de Compostela, 15782, Santiago de Compostela, Spain. E-mail: martin.fananas@usc.es*

[c]*School of Chemistry, University of Manchester, Oxford Road, Manchester M13 9PL, UK*

† Electronic supplementary information (ESI) available. CCDC 2131105. For ESI and crystallographic data in CIF or other electronic format see DOI: https://doi.org/10.1039/d2sc05192c

‡ E. M. C. and M. D. contributed equally to this work.

COFs;[23] this can also lead to the formation of subnanometer clusters with superior catalytic performances, in comparison with standard Pd catalysts,[24,25] but reduced porosity is still obtained due to the bulky organic complexes which limit the accessibility to the Pd centres. These problems can be circumvented by the incorporation of Pd as metal nodes (Fig. 1c), *i.e.*, the formation of a Pd-MOF in which the Pd atoms form part of the framework. These can be prepared by direct synthesis[26] or, as demonstrated recently, by transmetallation.[27]

These MOFs feature accessible Pd(II) sites, but the stability of the framework is compromised during the catalysis, as changes in the coordination sphere of the Pd centres cause rupture of the framework. A facile solution is the incorporation of the Pd centres as part of the ligands, *i.e.* using a metalloligand to connect the metal nodes, thus resulting in a framework with two different secondary building blocks (Fig. 1d). This was shown to be successful by Trikalitis and co-workers, who combined a Pd metalloligand with an indium trimer producing a 3D MOF, although with limited stability in solvents.[28] With this approach, a more uniform distribution of the Pd centres along the material is thus achieved with no blockage of the pores. This could also reduce the instability of the framework caused by the change in the coordination sphere during catalytic cycles. However, this has rarely been achieved through the conventional synthetic methodologies,[28,29] due to the tendency of Pd(II) to be reduced under these conditions, except for metalloligands where the Pd(II) centres are very inert, and thus, not useful in catalysis.

In this work, we use a solvent-assisted reaction to prepare a robust heterometallic MOF constructed by triangular $[Fe_3(\mu_3O)(COO)_6]^+$ secondary building units linked by square-planar Pd(II) centres. Structure solution through single crystal X-ray diffraction reveals a cubic system isoreticular to the well-known MIL-127, with pores of 2509 $Å^3$ which are available as confirmed by N_2, CO_2 and CH_4 sorption studies, with a BET area of 710 $m^2\ g^{-1}$. The stability studies of this MOF reveal excellent results across wide ranges of pH, temperatures, and solvents which allow its implementation in catalysis. Finally, studies on the catalytic activity of this heterometallic MOF towards the Suzuki–Miyaura allylation of different boronic acid pinacol esters show that this MOF is an efficient catalyst for $C(sp^3)$–$C(sp^3)$ and $C(sp^2)$–$C(sp^3)$ couplings.

Results and discussion

In order to demonstrate a better control on the formation of a heterometallic MOF, a mixture of the commercial cluster $[Fe_3O(CH_3COO)_6]ClO_4$ was reacted with the preformed palladium metalloligand $PdCl_2(H_2PDC)_2$ (H_4L, where H_2PDC = pyridine-3,5 dicarboxylic acid). In contrast to the common approach in the preparation of MOFs, this reaction was performed in the absence of a large amount of solvent, as we have previously used for the synthesis of the elusive Fe(II) analogue of ZIF-8,[30] but in the presence of only a small amount of acetic acid (20 microliters for 0.04 mmol of palladium metalloligand). The mixture was sealed under vacuum in an ampoule and heated at 170 °C for 48 h, resulting in the formation of red cubic crystals of formula $[Fe_3O(L)_{1.5}(H_2O)_2(OH)]\cdot$solvent (denoted as **MUV-22**), very small but of suitable quality for structure determination *via* single-crystal X-ray diffraction (Fig. 2 and Section S2 in the ESI†). The use of a small amount of acetic acid, analogous to the solvent-assisted mechanochemical approach,[31] is essential for the exclusive formation of **MUV-22**, which is the iron analogue of the reported $[In_3O(L)_{1.5}(H_2O)_2Cl]\cdot n(solv)$.[28]

A larger amount of acetic acid yields a mixture of phases, with the formation of a polymorph of **MUV-22**.[32] Very recently, Horike *et al.* have reported that solvent-free reactions with carboxylates require the formation of co-crystals,[33] although we show here an alternative route through the use of a minor amount of solvent. Importantly, this methodology yields

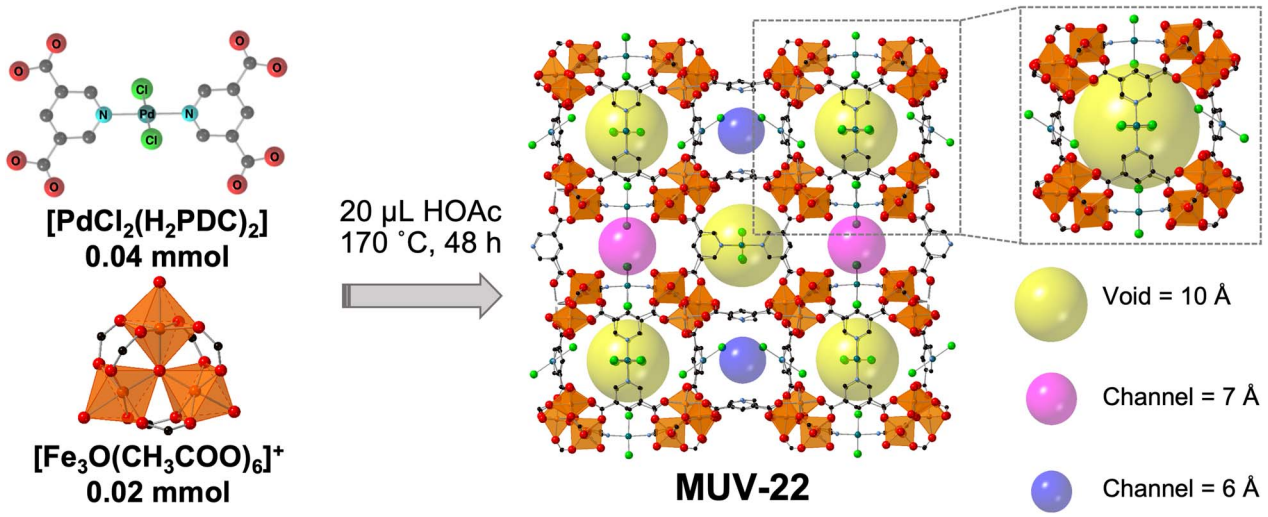

Fig. 2 Scheme of the chemical reaction between the metalloligand $PdCl_2(H_2PDC)_2$ and $[Fe_3(\mu_3O)(CH_3COO)_6]^+$ to produce **MUV-22** (colour scheme: orange = Fe, black = C, blue = N, red = O, dark teal = Pd, green = Cl; hydrogen atoms have been omitted for clarity). Details of the cuboidal cage are shown inside the discontinuous square. The large yellow spheres represent the cavity size, and pink and blue the channels.

a highly crystalline material which is phase pure, as confirmed by PXRD (Fig. S3†). The bulk material was exhaustively washed with a large amount of EtOH, immersed in the solvent overnight in order to remove any unreacted starting material and the acetic acid, and finally, heated at 120 °C under vacuum overnight. The infrared (IR) spectra of the powder confirmed the absence of any unreacted starting material (Fig. S4 and S5†).

Single-crystal X-ray diffraction analysis of the as-synthesized material reveals that the red cubic crystals, shown in Fig. 3a, are isostructural with MIL-127,[34] crystallizing in the space group $Pm\bar{3}n$, with unit cell parameters of $a = b = c = 22.1118$ Å (Table S1†). Structure solution reveals the presence of 6-connected trimeric $[Fe_3(\mu_3O)(COO)_6]^+$ SBUs and tetratopic $[PdCl_2(PDC)_2]^{4-}$ metalloligands. Thus, each $Fe_3O(COO)_6$ unit acts as a six-connected node, whereas each metalloligand acts as a four-connected node, resulting in the construction of a (4,6)-connected structure with the augmented *soc* network (Fig. 2). The net is composed of a periodic arrangement of one kind of cages with a diameter of 10 Å (yellow spheres in Fig. 2) and two different channels with approximate diameters of 6–7 Å (pink and blue spheres in Fig. 2). The Pd metalloligands are located at the faces of a cube and connect the eight corners occupied by Fe_3O trimers, each of which can be considered as a 6-c node with a trigonal prismatic geometry. Each metalloligand is composed of one palladium center coordinated by two Cl^- (each disordered over two positions) and two pyridine moieties. X-ray photoelectron spectroscopy (XPS) confirms the oxidation state of the palladium ions in **MUV-22** (Fig. 3b), with binding energies representative of Pd(II) (Pd $3d_{5/2}$ = 337.9 eV and Pd $3d_{3/2}$ = 343.6 eV),[35] and absence of Pd(0).

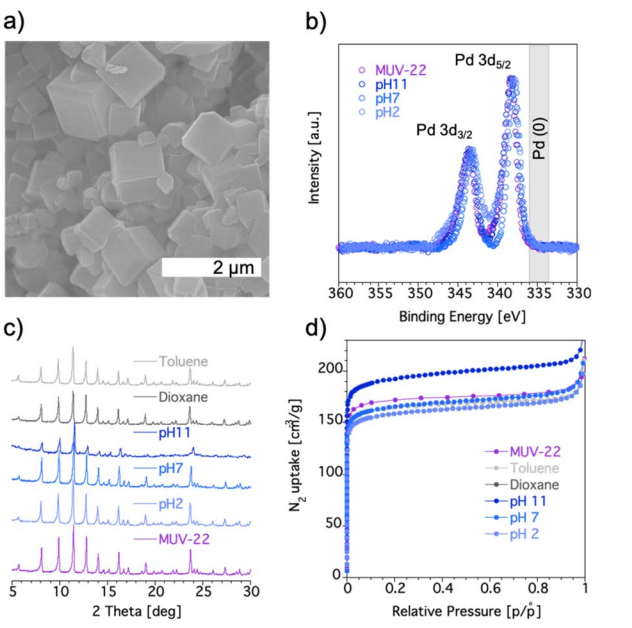

Fig. 3 (a) SEM image of **MUV-22** crystals; (b) XPS spectra of **MUV-22** showing the absence of Pd(0) after different treatments; (c) PXRD patterns of **MUV-22** after different treatments; (d) N_2 adsorption isotherms of **MUV-22** at 77 K before and after immersion in different solvents and pH aqueous solutions.

Thermogravimetric analysis (TGA) of washed **MUV-22** exhibits a sharp mass loss of 20% between 25 and 50 °C, and a large plateau above 200 °C until the final decomposition at 310 °C, thus showing an expected thermal stability (Fig. S8†).

To examine the chemical stability of **MUV-22**, it was immersed for 24 h in different aqueous solutions with pH values ranging from 2 to 11 and in different organic solvents. The PXRD patterns of the recovered materials reveal that crystallinity is maintained under these conditions (Fig. 3c), in sharp contrast to the indium analogue, which is unstable both in organic solvents and H_2O.[28] Additionally, the possible degradation of the MOF was investigated examining the supernatant solution by ^1H NMR spectroscopy, in order to detect the possible presence of organic ligands after 24 h immersion of **MUV-22** in deuterated dioxane, toluene and different deuterated aqueous solutions of pH range between 1 and 11. As shown in Fig. S12,† no signal of the pyridine-3,5-dicarboxylic acid could be detected. Furthermore, the solid used in each treatment was also studied by measuring: (a) the porosity from N_2 adsorption isotherms at 77 K, showing no significant reduction of the sorption capacity (Fig. 3d); and (b) the valence state of palladium by XPS to discard the formation of Pd(0) (Fig. 3b).

The porous nature of **MUV-22** was assessed by N_2 sorption at 77 K. Activation of **MUV-22** was successfully achieved by treating the washed material at 120 °C overnight. Fig. 3d displays the N_2 adsorption isotherm, a typical type I isotherm with a plateau at 180 $cm^3\ g^{-1}$. The obtained accessible surface area was calculated using the Brunauer–Emmett–Teller (BET) model, giving a value of 710 $m^2\ g^{-1}$ which is comparable with the reported values of the In analogue MOF (795 $m^2\ g^{-1}$),[28] and a pore volume of 0.323 $cm^3\ g^{-1}$. The pore size distribution was calculated using the corrected Horvath–Kawazoe method,[36] exposing a narrow distribution of microporosity (4.6–5.39) Å with the maximum peak at 4.85 Å. The CO_2 and CH_4 gravimetric sorption isotherms, shown in Fig. S15 and S16,† reveal a total uptake of 7.2 and 4.8 mmol g^{-1} at 18 bar, respectively. The isosteric heats of adsorption (q_{st}) were calculated through the Clausius–Clapeyron equation, resulting in 22.6 kJ mol^{-1} (for CO_2) and 15.1 kJ mol^{-1} (for CH_4), highlighting a higher affinity of **MUV-22** toward carbon dioxide (see Fig. S17†). These values are slightly smaller than those found in $[In_3O(L)_{1.5}(H_2O)_2Cl]$ (29.8 and 19.6 kJ mol^{-1} for CO_2 and CH_4, respectively), indicating a weaker interaction of the framework with the gas likely due to the use of a different metal.[28]

Given the high chemical stability of **MUV-22**, its porous nature, and the easy accessibility to the Pd(II) centers, we investigated its catalytic activity in allylic alkylation reactions. Pd-catalyzed allylic alkylation represents a highly versatile tool in chemical synthesis and has been used in the preparation of many natural products and biologically active compounds.[37] Although it has been extremely useful for the construction of C–C bonds using several organometallic reagents such as organoaluminum or Grignard reagents,[38] the Pd-catalyzed allylation of alkylboron compounds has been rarely reported.[39] Consequently, we decided to explore the catalytic activity of **MUV-22** in the reaction between methylboronic acid pinacol ester (**1a**), a typically reluctant reagent in cross-coupling reactions, and

Table 1 Comparison of the catalytic activity of **MUV-22** and related systems in the coupling between methylboronic acid pinacol ester and cinnamyl bromide

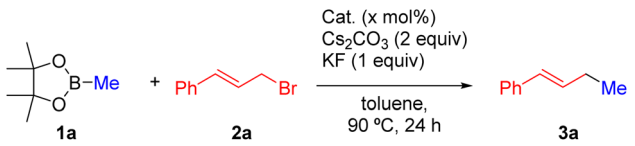

1a **2a** **3a**

Entry	Cat (x mol%)	Conversion (%)	**3a** (%)
1	**MUV-22** (2.5%)	Full	58
2	—	75	—
3	$Pd(OAc)_2$ (10%)	Full	20
4	$Pd(OH)_2/C$ (2.5%)	Full	43
5	Pd-PEPPSI-IPr (2.5 mol%)	Full	41
6	$PdCl_2(H_2PDC)_2$ (2.5%)	Full	42
7	$[Fe_3O(OAc)_6](ClO_4)$ (1.7%)	87	18
8	$PdCl_2(H_2PDC)_2$ (2.5%) $[Fe_3O(OAc)_6](ClO_4)$ (1.7%)	Full	41

cinnamyl bromide (**2a**). After screening of several reaction parameters (see the ESI, Tables S2–S4†), we found that **MUV-22** efficiently promotes the reaction in the presence of Cs_2CO_3 and KF in toluene at 90 °C (Table 1, entry 1). Under these conditions, (*E*)-1-phenyl-1-butene (**3a**) was cleanly formed in 58% yield.[40] Importantly, product **3a** was not formed in the absence of a catalyst (entry 2). In addition, **MUV-22** shows better catalytic performance than homogeneous $Pd(OAc)_2$ (entry 3), heterogeneous $Pd(OH)_2/C$ (entry 4) or even Pd-PEPPSI-IPr (entry 5) which is the state-of-the-art catalyst for the homogeneous Pd-catalyzed coupling between allyl bromides and alkyl boronic esters.[39]

To check a possible cooperative bimetallic effect in **MUV-22** in which the Fe atom might activate the allylic substrate *via* Lewis acid catalysis,[41] we carried out several control experiments using the corresponding Pd and Fe monomers and a combination of both (entries 6–8). The reaction took place in the presence of Pd monomer, although **3a** was obtained in a diminished yield (entry 6). The Fe monomer also showed some catalytic activity, but the coupling product was formed in a much lower yield (entry 7). Interestingly, combination of both monomers led to a similar result than the one obtained for the Pd monomer, providing the coupling product in lower yield than the one obtained with **MUV-22** (entry 8). Although bimetallic catalysis cannot be discarded at this point, these results suggest that the superior catalytic activity of **MUV-22** might be due to a structural confinement effect. Furthermore, comparison of the catalytic activity in the coupling of Me-Bpin with a larger substrate (*i.e.* (*E*)-2-(3-bromoprop-1-en-1-yl) naphthalene) demonstrates a more drastic difference in selectivity (45% yield with **MUV-22** *vs.* 18% yield with the mixture of the monomers).

Having established optimized conditions, we set out to explore the scope of this transformation (Scheme 1). **MUV-22** proved to be an efficient catalyst for the coupling of a range of allyl bromides bearing aromatic groups with electronically

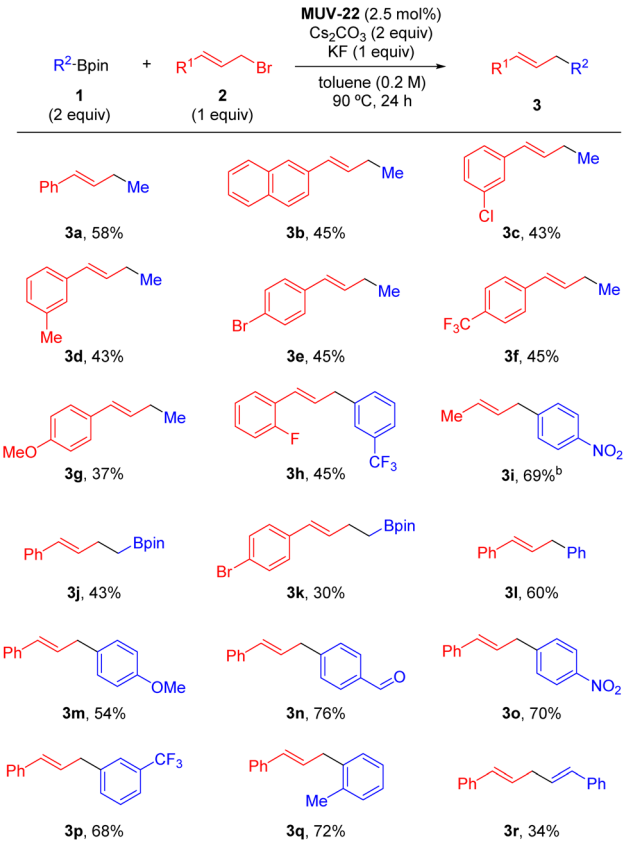

Scheme 1 Scope of the **MUV-22** catalyzed Suzuki–Miyaura allylation. [a]Reaction conditions: **1** (0.4 mmol), **2** (0.2 mmol), **MUV-22** (2.5 mol%), Cs_2CO_3 (0.4 mmol), KF (0.2 mmol), toluene (1 mL). Yield values refer to isolated products [b]obtained as a 2 : 1 mixture of linear : branched regioisomers.

distinct substituents at different positions (**3a–3h**). Crotyl bromide was also an efficient coupling partner although in this case product **3i** was obtained as a 2 : 1 mixture of regioisomers. Other alkyl boronic esters such as diborylmethane could be used as illustrated with the synthesis of homoallylboronates **3j** and **3k**. However, alkyl-Bpin reagents bearing hydrogen atoms in the β-position did not undergo this transformation likely due to competitive β-hydride elimination pathways (see Section S6.6 in the ESI†). **MUV-22** also proved to be an efficient catalyst for the allylation of C(sp^2) nucleophiles. In this context, Ph-Bpin (**3l**) and other aryl boronic esters bearing *para*- (**3m–3o**), *meta*- (**3p**) and *ortho*-substituted rings (**3q**) were coupled with cinnamyl bromide in good yields. Additionally, the skipped diene **3r** could also be synthesized under **MUV-22** heterogeneous catalysis conditions by using the corresponding alkenyl boronic ester.

Recycling experiments of **MUV-22** showed that the MOF still had remarkable catalytic efficiency after 4 cycles. Kinetic studies (Fig. 4a) revealed that the rate and yield of the reaction are essentially maintained between these runs, which demonstrates that **MUV-22** is robust and maintains its activity. Furthermore, we analyzed the chemical stability of the MOF recovered after the catalysis, *i.e.* **MUV-22-PC** (see Section S7 in

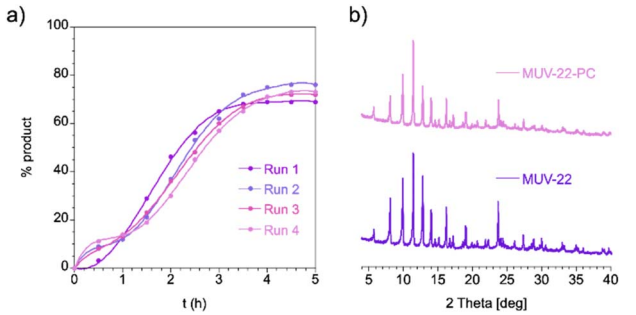

Fig. 4 (a) Recycling of MUV-22 in the formation of product 3l; (b) PXRD patterns of MUV-22 and MUV-22-PC.

the ESI†). PXRD studies revealed that the crystallinity of the MOF is maintained in the recovered catalyst (Fig. 4b), as also its porous nature (Fig. S62†). The particle morphology and crystal sizes were examined through SEM (Fig. S60†) and TEM (Fig. S61†) revealing similar results for **MUV-22** and **MUV-22-PC**, discarding in the last one the formation of nanoparticles. However, EDS studies showed that Cl^- ions were replaced by F^- ions in the coordination sphere of the Pd atoms (Fig. S59†), which was also confirmed with XPS (Fig. S58†). Interestingly, mixing of **MUV-22** with KF in toluene at 90 °C did not result in such a process (Fig. S63†). These results suggest that this Cl/F ligand exchange might occur in some of the Pd intermediates that are generated during the catalytic cycle,[42] further indicating that the reaction happens in the inside of the MOF crystal. In addition, although a possible Pd–N bond cleavage cannot be ruled out, the absence of Pd(0) by XPS (Fig. S57†) suggests a non-dissociation of the metalloligand, in agreement with previous studies from Amatore, Jutand and others.[43]

Finally, the coupling between (4-formylphenyl)boronic acid pinacol ester and cinnamyl bromide (*i.e.* formation of **3n**) was used to test the heterogeneous nature of the catalyst, through a leaching test based on a hot filtration experiment (see section S6.4 in the ESI† for details). Treatment of the filtrate with more Cs_2CO_3 under the same reaction conditions did not lead to any further formation of the product, thus establishing that no palladium leaches out of the MOF and excluding any homogeneous pathway.

Conclusions

In conclusion, we have shown a solvent-assisted reaction to incorporate accessible Pd(II) centres in the framework of a novel MOF, denoted as **MUV-22**, using a Pd-metalloligand. The regular disposition of the Pd(II) atoms, combined with the high chemical stability and the available space provided by the porous framework, makes **MUV-22** an interesting material for catalytic applications. In this sense, the activity of **MUV-22** in the Suzuki–Miyaura allylation has been explored. We have observed that this material acts as an efficient heterogeneous catalyst for the C–C bond formation between a range of alkyl, aryl and alkenyl boronates with different allyl bromides. We have shown that **MUV-22** catalyzes this reaction maintaining the crystallinity and the activity for several cycles. The robustness of this Pd/Fe MOF, combined with its high catalytic activity, paves the way for new opportunities in heterogeneous catalysis. Therefore, this is an example of how mixed-metal MOFs offer the possibility of incorporating multiple functionalities and take MOFs into account as heterogeneous catalysts.[44] Further studies on its use in other cross-coupling reactions are currently underway.

Experimental

Synthesis of MUV-22

MUV-22 was synthesized using a solvent-assisted method. $[Fe_3O(CH_3COO)_6](ClO_4)\cdot nH_2O$ (14 mg, 0.020 mmol) and *trans*-$[Pd_2Cl_2(H_2PDC)_2]$ (20 mg, 0.039 mmol) were initially briefly grounded. The mixture was placed in a glass tube and acetic acid (20 μL, 0.350 mmol) was added. The tube was flash-frozen with liquid nitrogen and sealed after a cycle of vacuum. Ten of such tubes were heated for 48 h at 170 °C (heating and cooling rates of 6 °C h^{-1}). The resulting mixture was washed with ethanol (3 × 25 mL) and then with methanol (6 × 25 mL) for 2 days. Yield: 140 mg (67%). Phase-purity was confirmed with X-ray powder diffraction, and the heavy atom element content was checked with EDS and ICP (calc. Pd : Fe : Cl ratio = 1 : 2 : 2; EDS: Pd : Fe : Cl ratio = 1.0 : 2.1 : 2.2; ICP: Pd : Fe ratio of 1.0 : 1.8).

Single crystal diffraction

X-ray data for compound **MUV-22** were collected with a Rigaku Supernova with microfocus Mo-Kα radiation at 120 K. Data were measured, processed and reduced using the CrysAlisPro suite of programs. Absorption correction was performed using empirical methods (SCALE3 ABSPACK) based upon symmetry-equivalent reflections combined with measurements at different azimuthal angles. The crystal structure was solved and refined against all F^2 values using the SHELX and Olex 2 suite of programmes. Despite the use of a highly intense X-ray source, crystals of **MUV-22** only diffracted to 1.25 Å of resolution. All atoms were refined anisotropically with the exception of carbon and nitrogen atoms in order to maximize the data/parameter ratio. Chloride atoms were found to be disordered and were modelled over two positions, where atomic distances were restrained using distance restrains. The atomic displacement parameters were restrained using rigid body restrains. Hydrogen atoms were placed at calculated positions. The solvent mask protocol in Olex 2 was used to account for the remaining electron density, finding 128 electrons per formula unit, which could correspond to 13 water molecules. CCDC 2131105 contains the supplementary crystallographic data for this paper.†

Gas sorption

MUV-22 crystals were activated at 120 °C under vacuum, overnight. Low-pressure single-gas nitrogen adsorption isotherms were measured in a Tristar II Plus sorptmeter (Micromeritics), at 77 K. High-pressure single-gas adsorption isotherms of CO_2

and CH_4 were recorded at different temperatures ranging from 283 to 333 K in an IGA-100 gravimetric gas sorption analyser (Hiden Isochema) using approximately 40 mg of **MUV-22**. Equilibrium conditions corresponded to 600 s interval and 0.001 mg min^{-1} tolerance.

Catalytic activity

General procedure. A 5 mL pressure tube equipped with a magnetic stirring bar was charged with **MUV-22** (2.5 mol%), Cs_2CO_3 (0.4 mmol), and KF (0.2 mmol). The corresponding acid pinacol ester (0.4 mmol) and the allyl bromide (0.2 mmol) were dissolved in toluene (0.8 mL and 0.2 mL, respectively) and subsequently added to the reaction vessel. The reaction mixture was stirred at 90 °C for 24 hours. Then, Et_2O (2 mL) was added, and the mixture was decanted. This was repeated 4 times. The combined organic layers were filtered through a pad of silica and the solvent was removed under vacuum. The crude product was purified by column chromatography over silica gel.

Data availability

The data that support the findings of this study are available in the ESI for this article.†

Author contributions

E. M.-C. and M. D. D. performed the synthesis and characterization of the MOF. E. M.-C. and V. F.-T. performed the catalysis experiments. I. J. V.-Y. contributed to solution and refinement of the structure from single crystal data. E. A. G. performed the gas sorption studies. M. F.-M. and G. M. E. supervised the project and wrote the manuscript, with input from all the authors.

Conflicts of interest

There are no conflicts to declare.

Acknowledgements

The work has been supported by the European Union (ERC-2016-CoG 724681-S-CAGE, ERC-CoG 863914-BECAME and European Regional Development Fund – ERDF), grants PID2020-117177GB-I00, and CEX2019-000919-M, funded by MCIN/AEI/10.13039/501100011033, the Generalitat Valenciana (Prometeo programme) and the Xunta de Galicia (ED431C 2022/27; Centro singular de investigación de Galicia accreditation 2019–2022, ED431G 2019/03). E. M.-C. and E. A.-G thank MICINN for a PhD fellowship (BES-2017-082451) and a Juan de la Cierva Formación fellowship (FJC2019-039015-I), respectively.

References

1 Q. A. Chen, Z. S. Ye, Y. Duan and Y. G. Zhou, *Chem. Soc. Rev.*, 2013, **42**, 497–511.
2 N. Miyaura and A. Suzuki, *Chem. Rev.*, 1995, **95**, 2457–2483.
3 B. Yan, L. Zhang, Z. Tang, M. Al-Mamun, H. Zhao and X. Su, *Appl. Catal., B*, 2017, **218**, 743–750.
4 Y. S. Kang, Y. Lu, K. Chen, Y. Zhao, P. Wang and W. Y. Sun, *Coord. Chem. Rev.*, 2019, **378**, 262–280.
5 M. Li, D. Posevins, A. Geoffroy, C. Zhu and J. Bäckvall, *Angew. Chem., Int. Ed.*, 2020, **59**, 1992–1996.
6 S. M. J. Rogge, A. Bavykina, J. Hajek, H. Garcia, A. I. Olivos-Suarez, A. Sepúlveda-Escribano, A. Vimont, G. Clet, P. Bazin, F. Kapteijn, M. Daturi, E. V. Ramos-Fernandez, F. X. I. Llabrés i Xamena, V. Van Speybroeck and J. Gascon, *Chem. Soc. Rev.*, 2017, **46**, 3134–3184.
7 A. Bavykina, N. Kolobov, I. S. Khan, J. A. Bau, A. Ramirez and J. Gascon, *Chem. Rev.*, 2020, **120**, 8468–8535.
8 A. Dhakshinamoorthy, A. M. Asiri and H. García, *Trends Chem.*, 2020, **2**, 454–466.
9 V. Pascanu, G. González Miera, A. K. Inge and B. Martín-Matute, *J. Am. Chem. Soc.*, 2019, **141**, 722–7234.
10 C. Xu, R. Fang, R. Luque, L. Chen and Y. Li, *Coord. Chem. Rev.*, 2019, **388**, 268–292.
11 A. Corma, H. García and F. X. Llabrés I Xamena, *Chem. Rev.*, 2010, **110**, 4606–4655.
12 H. Furukawa, K. E. Cordova, M. O'Keeffe and O. M. Yaghi, *Science*, 2013, **341**, 1230444.
13 H. Li, M. Eddaoudi, M. O'Keeffe and O. M. Yaghi, *Nature*, 1999, **402**, 276–279.
14 H.-C. Zhou, J. R. Long and O. M. Yaghi, *Chem. Rev.*, 2012, **112**, 673–674.
15 F. R. Fortea-Pérez, M. Mon, J. Ferrando-Soria, M. Boronat, A. Leyva-Pérez, A. Corma, J. M. Herrera, D. Osadchii, J. Gascon, D. Armentano and E. Pardo, *Nat. Mater.*, 2017, **16**, 760–766.
16 L. Chen, Z. Gao and Y. Li, *Catal. Today*, 2015, **245**, 122–128.
17 Z. Wang and S. M. Cohen, *Chem. Soc. Rev.*, 2009, **38**, 1315–1329.
18 S. Mandal, S. Natarajan, P. Mani and A. Pankajakshan, *Adv. Funct. Mater.*, 2021, **31**, 2006291.
19 G. Lu, S. Li, Z. Guo, O. K. Farha, B. G. Hauser, X. Qi, Y. Wang, X. Wang, S. Han, X. Liu, J. S. DuChene, H. Zhang, Q. Zhang, X. Chen, J. Ma, S. C. J. Loo, W. D. Wei, Y. Yang, J. T Hupp and F. Huo, *Nat. Chem.*, 2012, **4**, 310–316.
20 S. Luo, Z. Zeng, G. Zeng, Z. Liu, R. Xiao, M. Chen, L. Tang, W. Tang, C. Lai, M. Cheng, B. Shao, Q. Liang and H. Wang, *ACS Appl. Mater. Interfaces*, 2019, **11**, 32579–32598.
21 X. Li, R. Van Zeeland, R. V. Maligal-Ganesh, Y. Pei, G. Power, L. Stanley and W. Huang, *ACS Catal.*, 2016, **6**, 6324–6328.
22 L. Chen, S. Rangan, J. Li, H. Jiang and Y. Li, *Green Chem.*, 2014, **16**, 3978–3985.
23 I. Romero-Muñiz, A. Mavrandonakis, P. Albacete, A. Vega, V. Briois, F. Zamora and A. E. Platero-Prats, *Angew. Chem., Inter. Ed.*, 2020, **59**, 13013–13020.
24 L. Liu and A. Corma, *Nat. Rev. Mater.*, 2021, **6**, 244–263.
25 R. Adam, M. Mon, R. Greco, L. H. G. Kalinke, A. Vidal-Moya, A. Fernandez, R. E. P. Winpenny, A. Domenech-Carbo, A. Leyva-Perez, D. Armentano, E. Pardo and J. Ferrando-Soria, *J. Am. Chem. Soc.*, 2019, **141**, 10350–10360.
26 F. X. Llabrés i Xamena, A. Abad, A. Corma and H. Garcia, *J. Catal.*, 2007, **250**, 294–298.

27 T. He, X.-J. Kong, J. Zhou, C. Zhao, K. Wang, X.-Q. Wu, X.-L. Lv, G.-R. Si, J.-R. Li and Z.-R. Nie, *J. Am. Chem. Soc.*, 2021, **143**, 9901–9911.
28 I. Bratsos, C. Tampaxis, I. Spanopoulos, N. Demitri, G. Charalambopoulou, D. Vourloumis, T. A. Steriotis and P. N. Trikalitis, *Inorg. Chem.*, 2018, **57**, 7244–7251.
29 V. Niel, J. M. Martinez-Agudo, M. C. Muñoz, A. B. Gaspar and J. A. Real, *Inorg. Chem.*, 2001, **40**, 3838–3839.
30 J. López-Cabrelles, J. Romero, G. Abellán, M. Giménez-Marqués, M. Palomino, S. Valencia, F. Rey and G. Mínguez Espallargas, *J. Am. Chem. Soc.*, 2019, **141**, 7173–7180.
31 G. A. Bowmaker, *Chem. Commun.*, 2013, **49**, 334–348.
32 M. D. Darawsheh, J. Mazarío, C. W. Lopes, M. Giménez-Marqués, M. E. Domine, D. M. Meira, J. Martínez, G. Mínguez Espallargas and P. Oña-Burgos, *Chem.–Eur. J.*, 2020, **26**, 13659–13667.
33 A. Hinokimoto, H. Izu, Y.-S. Wei, T. Nakajo, R. Matsuda and S. Horike, *Cryst. Growth Des.*, 2021, **21**, 6031–6036.
34 H. Chevreau, A. Permyakova, F. Nouar, P. Fabry, C. Livage, F. Ragon, A. Garcia-Marquez, T. Devic, N. Steunou, C. Serre and P. Horcajada, *CrysEngComm*, 2016, **18**, 4094–4101.
35 J. F. Moulder, W. F. Stickle, P. E. Sobol and K. D. Bomben, in *Chastain*, Perkin-Elmer Corporation, 1992.
36 L. S. Cheng and R. T. Yang, *Adsorption*, 1995, **1**, 187–196.
37 B. M. Trost and M. L. Crawley, *Chem. Rev.*, 2003, **103**, 2921–2944.
38 E. Negishi and L. Fang, in *Handbook of Organopalladium Chemistry for Organic Synthesis*, ed. E. Negishi, Wiley, New York, 2002, vol. 1, ch. III.2.9.
39 K. Endo, T. Ohkubo, T. Ishioka and T. Shibata, *J. Org. Chem.*, 2012, **77**, 4826–4831.
40 Moderate yield is likely due to volatility of the product.
41 For an example of Lewis acid activation in transition metal-catalyzed allylic substitution, see: E. Rivera-Chao, M. Mitxelena, J. A. Varela and M. Fañanás-Mastral, *Angew. Chem., Int. Ed.*, 2019, **58**, 18230–18234.
42 L. Grimaund and A. Jutand, *Synthesis*, 2016, **49**, 1182–1189.
43 C. Amatore, G. Le Duc and A. Jutand, *Chem.–Eur. J.*, 2013, **19**, 10082–10093.
44 M. Viciano-Chumillas, X. Liu, A. Leyva-Pérez, D. Armentano, J. Ferrando-Soria and E. Pardo, *Coord. Chem. Rev.*, 2022, **451**, 214273.